Surveys in Geophysics
https://doi.org/10.1007/s10712-026-09948-5

Effect of the Generation of Bouguer Anomalies on the Geoid Determination: A Case Study in a High-Mountainous Area

Ramazan Alpay Abbak[1] · **Kurt Seitz**[2]

Received: 21 November 2025 / Accepted: 24 February 2026

Abstract
Different types of gravity anomalies are engaged in geophysical and geodetic tasks. Whether they are used for regional or global applications, they require efficient calculations. All variants are based on the so-called free-air gravity anomalies. Mean free-air gravity anomalies on an equidistant grid are needed for gravity field modeling. Three possible ways of compiling mean free-air gravity anomalies are discussed in detail. One method is via simple Bouguer gravity anomalies, the second, more time-consuming method is via complete Bouguer gravity anomalies, and the third method is via topographic-isostatic reductions, which is a tedious task. In flat areas, the differences between using any of the three methods should not be significant. However, in mountainous regions, each dependency can negatively affect the interpolation process of gravity anomalies. The reduced gravity anomalies should be as smooth as possible in order to minimize the interpolation error which is inherent in the interpolation of the information in the arbitrarily distributed gravity observation points to obtain block average signals. This study investigates the effects of Bouguer and topographic-isostatic reductions on the accuracy of the mean gravity anomalies and the resulting gravimetric geoid model. The numerical results indicate that complete Bouguer approximations improve the accuracy of the geoid model by a few millimeters. Therefore, this method should be used to predict mean gravity anomalies, especially in mountainous regions, in few of the 1 cm geoid determination.

Keywords Colorado test-bed · Simple Bouguer · Complete Bouguer · KTH method · Tesseroid · Topographic-isostatic model

Article Highlights

- Reviewing the computational scheme of smoothing methods on geoid modelling.
- Introducing the input data as well as gridding the terrestrial gravity anomalies.

✉ Ramazan Alpay Abbak
raabbak@ktun.edu.tr

Kurt Seitz
kurt.seitz@kit.edu

[1] Department of Geomatics Engineering, Konya Technical University, Konya, Türkiye

[2] Geodetic Institute, Karlsruhe Institute of Technology, Karlsruhe, Germany

- Comparing the mean free-air gravity anomalies obtained from each method.
- Evaluating geoid models by control benchmarks in the absolute and relative sense.

1 Introduction

The geoid can, apart from marine topography, be equated with the mean sea level and extended inside the visible topographic masses. Since the geoid is a reference surface for physical heights (i. e. orthometric height), the height of points and depth of seabeds are directly measured from it. Thus, a precise geoid determination is essentially important for engineering studies and geoscientific purposes.

Nowadays, a precise geoid model can be determined using Stokes's formula (Heiskanen and Moritz 1967) together with gravity anomalies from terrestrial measurements and a global geopotential model (GGM). Various aspects related to the precise determination of the geoid are discussed (Sansò and Rummel 1997). The need for reductions in geoid determination is generally questioned, as it is carried out within the framework of the remove-compute-restore (RCR) method (Sjöberg 2009). Effects that are reduced from the free-air anomaly are corrected again in the restore step, according to the argumentation. Based on the Stokes theory, and the previously mentioned spectral decomposition, several gravimetric geoid determination methods have been offered by scholars since the 1990s, each of them has their own advantages and disadvantages. One of them is the KTH (Kungliga Tekniska Högskolan) method, which is successfully applied in several regions where a gravimetric geoid model is needed and the input data is available with high resolution and precision (see for mathematical details of the KTH method in Sjöberg 1984, 1991, 2003). The KTH approach has been proven to be a practical method that gives very precise geoid results. Several comparisons with other methods (e. g. Ågren et al. 2009) have shown very good performance. Thus, we use the KTH method to the geoid determination in this study. The aim of this study is to examine the pre-processing of the input data (smoothing, interpolation, etc.) and to identify possible optimization aspects. In the KTH method, mean gravity anomalies obtained from terrestrial point-gravity data are stochastically combined with gravity anomalies obtained from a truncated satellite-only GGM. Before this combination, a rigorous process is needed for the preparation of terrestrial gravity anomalies because they are important input data that mostly affect the accuracy of the geoid model.

In the preparation step, gridded gravity anomalies should be constructed for an efficient numerical evaluation of the Stokes integral. Thus, gravity observations taken at randomly distributed points on the Earth's topography are reduced to the geoid, which acts as the boundary surface of the problem. Furthermore, it is assumed that atmospheric and tidal reductions have already been incorporated into the measured values. As a result, all masses outside the boundary surface must be eliminated by suitable reductions. This theoretical requirement for the boundary values is achieved through the free-air reduction and the topographic-isostatic reduction. Comparing these down-ward continued values with normal gravity on the reference ellipsoid results in the Bouguer gravity anomaly. Then they should be interpolated to mean values assigned to grid centres (centre of cell) using a precise interpolation technique. There are two types of Bouguer anomalies: simple and complete (Hofmann-Wellenhof and Moritz 2006). Simple Bouguer anomaly is preferred in flatter areas for smoothing gravity due to its practical calculation, whereas the complete Bouguer anomaly is inevitable in mountainous areas. Another rigorous option for the smoothing gravity is the topographic-isostatic reduction. However, it is a very difficult and cpu-time

consuming task to compute this reduction. Recently, topographic-isostatic models in terms of spherical harmonic coefficients have been released (e. g. Grombein et al. 2014a) and become available on the ICGEM webpage (https://icgem.gfz-potsdam.de). These models are subject to analysis in the prediction of mean gravity anomalies and resulting geoid model.

In the geosciences, there is a very limited number of studies that investigate the effect of smoothing methods on the prediction of mean gravity anomalies and their impact on the accuracy of geoid determination. Firstly, Featherstone and Kirby (2000) compare direct (free-air) and simple Bouguer anomalies for smoothing gravity across the continental Australia. It is found that the minimum and maximum differences between gravity anomalies derived from free-air (aliased) and simple Bouguer (non-aliased) grids are 77 mGal and −84 mGal, respectively. Those differences affects the geoid heights more than 2 m over Australia. Then, Goos et al. (2003) research the effect of the gridding of simple and complete Bouguer anomalies prior to the computation of regional gravimetric geoid models over Australia. It is outlined that there are no significant differences between both methods over Australia in the accuracy achieved for the geoid due to low topography. Subsequently, Vaníček et al. (2004) offer the spherical shell instead of planar plate while computing Bouguer gravity anomalies. Finally, Janák and Vaníček (2005) compare both simple and complete approximations for gridding gravity anomalies in Rocky mountains, Canada. It is concluded that mountainous areas require complete Bouguer approximation in smoothing gravity.

According to the literature mentioned above, no paper concentrates the effect of topographic-isostatic reduction on the smoothing gravity anomalies by comparing Bouguer anomalies, and there is not available a comprehensive study that compares the planar, spherical, spherical cap, and tesseroidal approximations. Thus, this study investigates how topographic-isostatic models as well as Bouguer approximations considering different type of the crust, affect the accuracy of the mean gravity anomalies, and resulting geoid model in a high-mountainous area. Hence, explaining the theoretical background of approximations, all approximations will be compared in Colorado test-bed (Wang et al. 2021) numerically.

This paper starts with an outline of three smoothing approximations for predicting mean gravity anomalies. Then, features of input datasets and their accuracy are explained for the extensive numerical investigations. Subsequently, several comparisons are made considering mean free-air gravity anomalies and the gravimetric geoid model in the absolute and relative sense. Afterwards, numerical results of our investigations are discussed. Lastly, the paper concludes by providing a summary of the outcomes and some recommendations.

2 Methods

Gravity values measured on the physical surface of the Earth are not directly included in the geoid determination. Therefore, gravity measurements require to be converted into different types of gravity anomalies (e. g. Jalal et al. 2022) or gravity disturbances (e. g. Abbak et al. 2022), depending on the application or considered boundary value problem. Most of the geodetic applications (Heck and Seitz 2003) use the gravity anomaly or disturbance as input for a integral solution. Subsequently, these gravity anomalies or gravity disturbances should be interpolated to grid centres, representing the mean value of the grid cell, in order to solve the respective integral numerically.

In the presented paper, we focus on the generation of those mean gravity anomalies, namely the free-air gravity anomalies which enter the Stokes integral in the KTH method. The subsidiary effects that occur in this context (non-linear effect, ellipsoidal effect, atmospheric effect, direct and indirect gravity effect, etc) are evaluated separately and applied as corrections to the solution of the Stokes integral. Their calculation is based on accepted standards (Heck 1988; Heck and Seitz 2003) and not investigated further.

Gravity information, which enters the interpolation process, should be as smooth as possible. Therefore, some reductions are applied to the free-air anomalies in the remove-step. After interpolation, the effects are restored to the gridded values. The results are gridded mean free-air anomalies, ready for the integration-step. In this context, free-air gravity anomalies are strongly correlated with the topographic masses. Thus, the topographic effects must be removed from free-air gravity anomalies before the interpolation. For this purpose, both the simple and complete Bouguer approximations as well as topographic-isostatic reductions can be employed (Hofmann-Wellenhof and Moritz 2006). In this study, all these approximations will be utilized for smoothing gravity anomalies. Finally, mean free-air gravity anomalies will be obtained by restoring topographic effects (i. e., the Bouguer effects and topographic-isostatic effect). This procedure is so-called remove-grid-restore method in geodetic literature, which is commonly confused by remove-compute-restore method to gravimetric geoid determination (Forsberg 1984; Forsberg and Tscherning 1997; Featherstone and Kirby 2000).

On the other hand, the KTH method, which has been applied in several geoid models of various countries, and accordingly with very different topographical conditions, will be operated for our geoid determination. Interested readers can be referred to Abbak and Ustun (2015) for theory and practical application of the method. Due to the limited space of the paper, we do not have the opportunity to outline the method here in detail.

2.1 Bouguer Anomalies

Firstly, the free-air gravity anomaly Δg^{FA} on the mean sea level is computed by

$$\Delta g^{FA} = g_P - \delta g^{FA} - \gamma_0, \tag{1}$$

where g_P is the observed gravity value at surface point P, γ_0 is the normal gravity on the reference-ellipsoid (Moritz 1980b). δg^{FA} is the effect of free-air, which is subtracted from g_P to get an predicted value from surface gravity measurement by assuming the vertical gravity gradient of the normal field as,

$$\delta g^{FA} = \frac{dg}{dh} \cdot H_P \doteq \frac{d\gamma}{dh} \cdot H_P = -0.3086 \cdot H_P, \tag{2}$$

where H_P (m) is the orthometric height of the gravity point P. In Eq. (2) the real vertical gradient of the gravity potential is approximated by the constant vertical gradient of the normal gravity with the value − 0.3086 (mGal/m). To calculate the latitude dependent normal gravity value on the surface of the reference-ellipsoid, Somigliana's formula (Somigliana 1929, 1930) can be exploited as:

$$\gamma_0(\varphi) = \gamma_a \frac{1 + k \cos^2 \varphi}{\sqrt{1 - e'^2 \cos^2 \varphi}}, \tag{3}$$

where γ_a is the normal gravity on the equator, k is a constant value, φ is the geodetic latitude of the point on the ellipsoid, e'^2 is the squared first numerical eccentricity of the

level-ellipsoid (Moritz 1980b). Table 1 presents some constants of GRS80 ellipsoid that used in this study.

In order to remove the effect of topographic masses, with the intention of smoothing the signal, the simple Bouguer gravity anomaly Δg^{SB} is calculated by,

$$\Delta \mathrm{g}^{\mathrm{SB}} = \Delta \mathrm{g}^{\mathrm{FA}} - 2\pi G \rho_0 H_{\mathrm{P}}, \tag{4}$$

where ρ_0 is the mean density of visible topographic masses, G is the Newtonian gravitational constant (cf. Table 1). Here the infinite planar Bouguer plate is assumed as approximation for the topography. However, a spherical shell can be also considered (Kadlec 2011, Eq. (2.148)) instead of the Bouguer plate. In this case Eq. (4) can be rewritten as,

$$\Delta g^{\mathrm{SB}} = \Delta g^{\mathrm{FA}} - 4\pi G \rho_0 H_P. \tag{5}$$

The potential effect of an ellipsoidal shell has been published by Seitz et al. (2023). It could also be handled as another model of the Bouguer plate.

In simple Bouguer anomalies, topographic masses are simplified as a planar plate, spherical cap or spherical shell. Their respective effect on gravity are:

$$\delta \mathrm{g}^{\mathrm{BP}} = \begin{cases} \text{Infinite planar plate:} & 2\pi G \rho_0 H_{\mathrm{P}}, P \text{ on the plate} \\ \text{Spherical shell:} & 4\pi G \rho_0 H_{\mathrm{P}}, P \text{ on the shell} \\ \text{Spherical cap:} & \text{see Heck and Seitz (2007, Eq. (54)),} \end{cases} \tag{6}$$

which are reduced (subtracted, cf Eq. (1)) from the free-air gravity anomaly.

However, the topography has variations from the planar plate or shell (their thickness is defined by the height H_{P} of the point P). Thus, the complete Bouguer (CB) anomaly $\Delta \mathrm{g}^{\mathrm{CB}}$, more rigorous approximation, takes the effect of the terrain (TC) into account

$$\Delta \mathrm{g}^{\mathrm{CB}} = \Delta \mathrm{g}^{\mathrm{FA}} - \delta \mathrm{g}^{\mathrm{BP}} - \delta \mathrm{g}^{\mathrm{TC}}, \tag{7}$$

where $\delta \mathrm{g}^{\mathrm{TC}}$ is the terrain effect (Hofmann-Wellenhof and Moritz 2006) which considers topographic undulation from the Bouguer plate or shell.

The masses of the terrain are considered up to a spherical distance ψ_{c}. This applies to both the remove step and the restore step. This is an advantage of the methodology, that

Table 1 Physical and geometrical constants in this study (Moritz 1980a)

Constant	Symbol	Value	Unit
Newton's Gravitational constant	G	6.6743×10^{-11}	$\mathrm{Nm^2\,kg^{-2}}$
Density of rocks	ρ_0	2670	$\mathrm{kgm^{-3}}$
Density of the mantle	ρ_{M}	3270	$\mathrm{kgm^{-3}}$
Mean thickness of the crust	T	30	km
Vertical gravity gradient	$\frac{\mathrm{d}\gamma}{\mathrm{d}h}$	− 0.3086	$\mathrm{mGalm^{-1}}$
Normal gravity on Equator	γ_a	9.7803267715	$\mathrm{m/s^2}$
Unitless value	k	0.001931851353	–
Square of the first eccentricity	e'^2	0.0066943800	–
Square of the second eccentricity	e^2	0.0067394968	–
Mean Earth radius	R	6371	km

remove and restore are carried out on the same functional compared to the RCR-method (Forsberg 1984; Forsberg and Tscherning 1997). The radius of the so-called Hayford zone O with $\psi_c = 1^\circ 29' 58''$ is the spherical distance. This corresponds to a lateral distance of 166.7 km (Heiskanen and Moritz 1967, Tab. 3-1).

In the calculation of complete Bouguer anomalies, the terrain effects is a tedious task for the geodesist and geophysicist because a high-resolution digital terrain model (DTM) must be evaluated in a 3-dimensional integral (Newton integral). Considering the discretization method of topographic structures, the computation of terrain effects are handled as prisms (Mader 1951; Nagy et al. 2002), cylinder (Marotta and Barzaghi 2017), and tesseroid (Heck and Seitz 2007). The computation process of the terrain effects needs a large hard-disk storage and faster processors in the computer environment, or parallel computing facilities. Generally, a special software package solely devoted the computation of TC is employed for this purpose (e. g. Forsberg and Tscherning 2014; Grombein et al. 2013; Goyal et al. 2020; Olgun et al. 2023).

On the other hand, considering the topography, we employ the constant density ρ_0 throughout the paper. Of course, the density issue is another important topic for gravimetric geoid determination (Kuhn 2003). For illustration, the effect of topographical density on the geoid in the Taurus Mountains (3524 m) can reach approximately 50 cm (Nergizci et al. 2024). However, in this paper we focus on different sources of errors.

2.2 Topographic-Isostatic Effect

Due to the availability of global high-resolution digital terrain models, it has now become possible to determine the gravitational effect of topographic masses on the Earth's gravity field. This is achieved through the technique known as Gravity Field Forward Modelling (GFFM), which is based on Newton's law of universal gravitation. GFFM provides the conversion of topographic mass into gravitational potential, again considering the assumption of the mean density of topographic masses ρ_0. As a isostatic model, the approach of Airy-Heiskanen (Heiskanen and Moritz 1967; Kuhn 2003; Sjöberg 1998, Chapter 3–4) is treated.

In the Colorado test area, all topographic heights are positive: $H > 0$ m. Therefore, the root below the mean crust of thickness $T = 30$ km is also positive: $t > 0$. H and t are related, based on the buoyancy equilibrium of topographic and isostatic masses for each DTM-element as

$$t = \frac{\rho_0}{\Delta\rho} \cdot H. \tag{8}$$

The positive density contrast between mantle and crust is indicated by $\Delta\rho = \rho_M - \rho_0$. If the isostatic masses are discretized by tesseroids, then the top surface of the tesseroid has a geocentric distance $r_2 = R - T$ and the bottom surface $r_1 = R - T - t$, respectively. The values used for the parameters involved are listed in Table 1.

The explained effects are benefited to generate point-wise reduced smooth gravity anomalies: simple Bouguer Δg^{SB}, complete Bouguer Δg^{CB} and isostatic anomalies Δg^{TI} which are additionally reduced by the isostatic effect δg^{I}. These smoothed anomalies are now interpolated on an equidistant grid. On this grid (i, j) the effects are restored as mean values, to have mean values prepared for numerical integration. As depicted in the flow chart supplied in Fig. 3, three types of gridded free-air gravity anomalies are obtained as follows:

free air anomalies based on the simple Bouguer reduction,

$$\Delta g_{ij}^{\mathrm{FA}} = \Delta g_{ij}^{\mathrm{SB}} + \delta g_{ij}^{\mathrm{BP}}, \tag{9}$$

free air anomalies based on the complete Bouguer reduction,

$$\Delta g_{ij}^{\mathrm{FA}} = \Delta g_{ij}^{\mathrm{CB}} + \delta g_{ij}^{\mathrm{BP}} + \delta g_{ij}^{\mathrm{TC}}, \tag{10}$$

and, free air anomalies including the isostatic effect,

$$\Delta g_{ij}^{\mathrm{FA}} = \Delta g_{ij}^{\mathrm{CB}} + \delta g_{ij}^{\mathrm{BP}} + \delta g_{ij}^{\mathrm{TC}} + \delta g_{ij}^{I}. \tag{11}$$

They enter the KTH method with the stochastically modified Stokes kernel function.

The respective terrain, topographic, and isostatic masses are discretized by the use of prisms (Mader 1951) and tesseroids (Heck and Seitz 2007; Grombein et al. 2013; Marotta et al. 2019) to compare these discretization methods.

3 Global Datasets

Global data sets which are used in geoid determination are described in this section, then the accuracy of the data sets is also addressed.

3.1 Global Topographic-Isostatic Model

The theory of the Rock-Water-Ice (RWI) approach has been developed to provide a more realistic modelling of Earth's topographic and isostatic masses, including continents, oceans, lakes, ice sheets and shelves, as well as isostatic compensation masses in the Earth's interior. Thus, the RWI model works with three different densities (rock, water and ice). The RWI approach is utilized to generate a series of topographic-isostatic (TOIS) gravity field models, which offer a high-resolution representation of Earth's topographic-isostatic gravitational potential in terms of spherical harmonics expanded up to degree and order 1800 (Release 2012). In this study, we will utilize the RWI_TOIS_2012 model (Grombein et al. 2014a) for our analysis. It is available on the ICGEM webpage (Ince et al. 2019).

3.2 Global Geopotential Model

The external gravitational field of the Earth is represented by solid spherical harmonics coefficients which are called Global Geopotential Model (GGM). Depending on the data to calculate the coefficients, GGMs are classified into three categories: satellite-only, combined and tailored models (Featherstone 2003). Nowadays, approximately 180 static GGMs were produced and released on the ICGEM (International Centre for Global Earth Models) webpage (Ince et al. 2019).

In the KTH method, satellite-only GGMs are preferred for the production of long-wavelength components in geoid determination in order to avoid the correlation between short wavelengths information and terrestrial data because the combined GGMs are highly correlated with terrestrial data. Thus, some recent satellite-only models (WHU-SWPU-GOGR2022S, Tongji-GMMG2021S, ITSG-Grace2018s, GOCO06s, IGGT_R1C) are

chosen for our investigations. After several spectral analyses such as degree variance, error degree variance, and etc., the IGGT_R1C model was decided to be used in this study. The model having complete degree and order 240, is produced from a combination of observations of the GOCE (Gravity field and steady-state ocean circulation explorer) and GRACE (Gravity Recovery and Climate Experiment) gravity field missions (Lu et al. 2018).

3.3 Global Digital Terrain Model

The physical Earth's surface is digitally represented by a DTM in the computer environment, which is essential for topographic corrections in geoid modelling studies. The Shuttle Radar Topography Mission (SRTM) has provided a high accuracy global DTM at one-arc-second resolution. The DTM was produced from a project which was jointly realized by NASA (National Aeronautics and Space Administration) and NGA (National Geospatial-Intelligence Agency) (Farr et al. 2007). Although it is defined that the global accuracy of the DTM is 16 m, its regional accuracy does not exceed 9 m (e. g. Bildirici et al. 2008). The vertical and horizontal datum of SRTM are EGM96 (Lemoine et al. 1998) and WGS84, respectively (Ustun et al. 2006; Bildirici et al. 2007). In this study, we will utilize the SRTM DTM at one-arc-second resolution (SRTM1) for calculation of the topographic and isostatic effects.

4 Numerical Investigations

In this section, the application of some smoothing technique across the Colorado test region prior to precise geoid determination are explained. The study area and input data are described by following with comparison of Bouguer approximations and topographic-isostatic model which will be engaged in prediction of mean gravity anomalies. Then, the geoid models considering different smoothing methods are compared with each other. Finally, new geoid models are assessed by means of GNSS (Global Navigation Satellite Systems)-levelling data in absolute and relative sense.

4.1 Study Area and Terrestrial Datasets

The Colorado test-bed is selected in this study because it was used for the comparison of several geoid modelling techniques such as LSMS, LSMH, UNB, and others (Işık et al. 2021; Wang et al. 2021). Hence, our study area is limited from 104° to 108° western longitudes, and from 36.5° to 38.5° northern latitudes, which covers approximately 80,000 km^2. The heights of the study area range from 1100 m to 4400 m, with a mean value of 2100 m. They are produced on a DTM with $1'' \times 1''$ resolution. This statistic means that the study area is one of the most complicated regions over the world from the point of view of topographic and geoidal variations. Furthermore, for efficiently evaluating the Stokes's integral, the mean elevations and gravity anomaly data are required in the nearest vicinity of the study area. Thus, the data area is extended at least by one degree in respect to the study area to avoid edge-effects. Hence, our data area is limited from 101.5° to 109.5° western longitudes, and from 35.5° to 39.5° northern latitudes, which covers approximately 320,000 km^2. At the southern east of the data area, the orthometric height decreases below 800 m. The topography of the study and data areas is displayed in Fig. 1.

The total number of gravity observations in the study area amounts to 59,303 produced by National Geodetic Survey of United States (CGE 2025). Each record contains the latitude, longitude, orthometric height and observed gravity value of a point *P*. The number of gravity points provides us a density of one point per 7 km^2, which is a lower density for a high precision geoid modelling study (Abd-Elmotaal et al. 2020). Outlier detection was already carried out by National Geodetic Survey. As a result, the accuracy of the data is better than 1 mGal. The spatial distribution of gravity surveys is displayed in Fig. 2.

The computed geoid models will be compared with a set of GNSS-levelling data since these are only independent data which verifies gravimetric geoid model on the land. The total number of available GNSS-levelling benchmarks in the study area is 223 (van Westrum et al. 2021). The geo-spatial distribution of the benchmarks is a east–west profile through the study area, as seen in Fig. 2. The horizontal accuracy of the points is at the mm level whereas the vertical accuracies of points are approximately estimated to be 1 and 2 cm for ellipsoidal and orthometric heights, respectively (van Westrum et al. 2021). This statistic means that the GNSS-levelling data offers us precise information on geometric geoid over the study area for a final point-wise assessment of the quality of the calculated geoid solution.

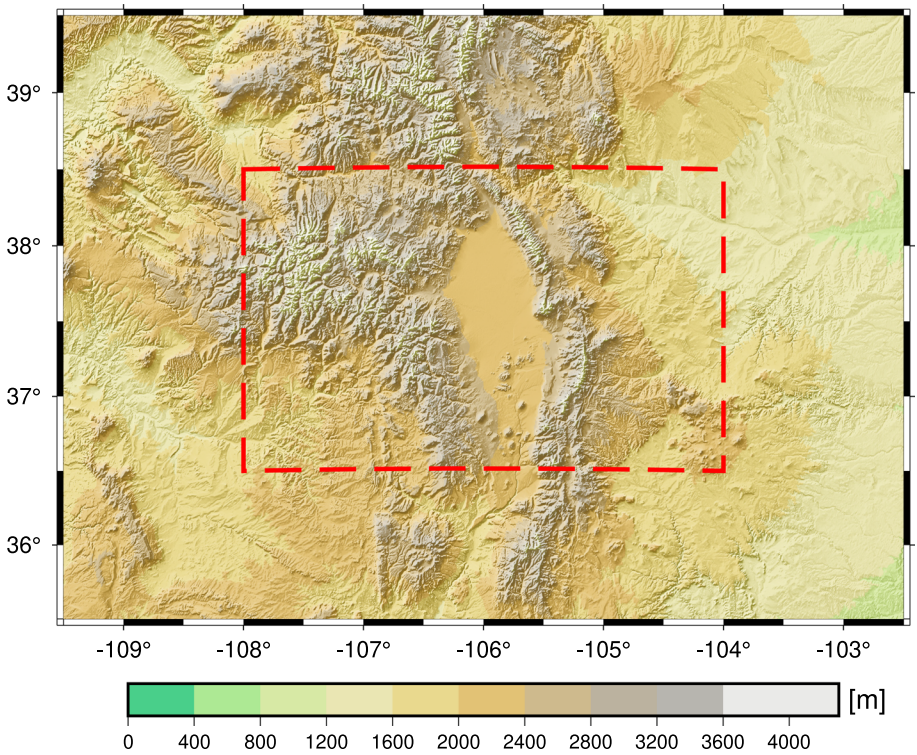

Fig. 1 The topography of the data area (dashed red line is the border of the study area)

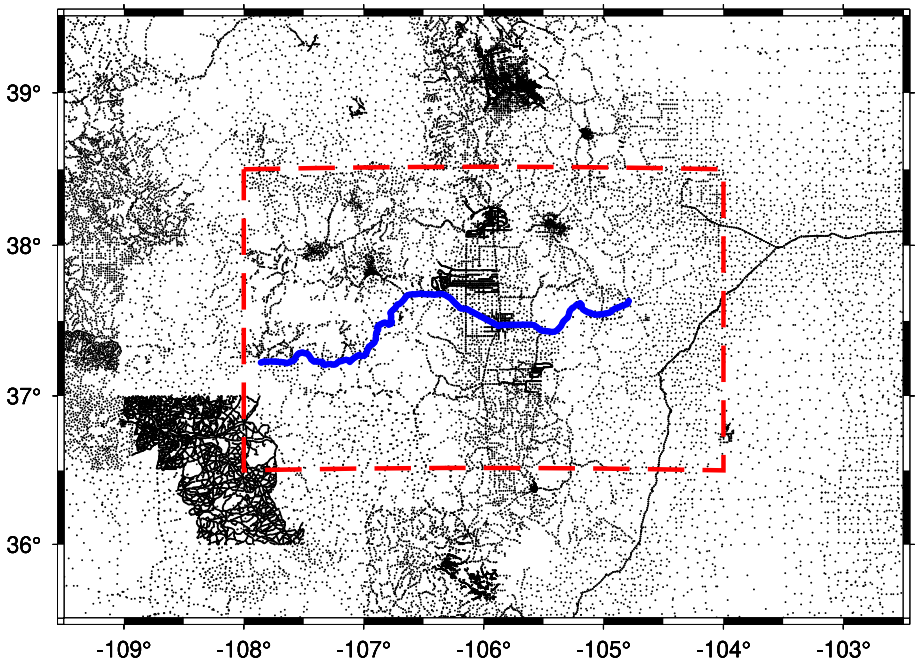

Fig. 2 The distribution of the terrestrial datasets over the study area (black dots are gravity surveys while blue dots are GNSS-levelling benchmarks)

4.2 Comparison of Free-Air Gravity Anomalies

Three types of smoothing methods provided three free-air gravity anomaly grids. The respective calculation process can be found in the flowchart in Fig. 3. The first algorithm of gridding gravity anomalies can be outlined as follows: free-air gravity anomalies randomly distributed on the surface of the Earth were converted to simple Bouguer anomalies Δg^{SB} using orthometric heights H_{P_i} of gravity points P_i. Then, using the nearest neighbour method, simple Bouguer anomalies were interpolated to the grid nodes. During interpolation, "nearneighbor" command of the GMT (Generic Mapping Tools) software (Wessel et al. 2019) was incorporated with options as maximum interpolation capsize equals to 12 arc-minutes as well as maximum and minimum numbers of points for each grid are 4 and 2, respectively. After the interpolation, simple Bouguer anomalies in grid centre were converted to free-air gravity anomaly grid by restoring the Bouguer plate effect via the mean height of every grid, which is produced by averaging all SRTM1 data in every grid cell. Hence, a free-air gravity grid Δg_{ij}^{FA} based on SB was reconstructed (cf Eq. (9)).

As the second gridding algorithm, simple Bouguer anomalies in points are converted to complete Bouguer (CB) anomalies Δg^{CB} by adding the terrain corrections at the gravity points. Then, using the same interpolation method and options, the complete Bouguer anomalies were transformed onto a regular grid. After interpolation, complete Bouguer anomalies in grid centres were converted to free-air gravity anomaly grid by adding the Bouguer plate effect via the mean height and restoring the mean terrain correction (cf. Eq. (10)). Hence, a free-air gravity grid based on CB was reconstructed. Here, the terrain

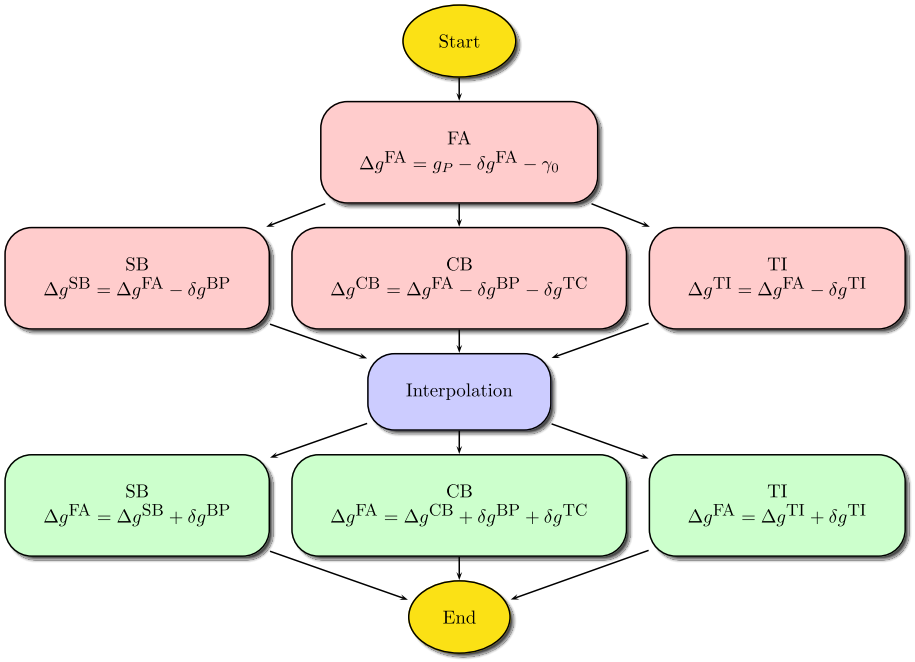

Fig. 3 Flowchart of all processes. The red frames denote computation of constituents at gravity points P whereas the green frames indicate computation of constituents at grid centres (i, j). While computing Bouguer plates (BP) in grid centre, the average heights are employed

corrections (TC) were prepared in two different ways to test whether the approximation method affects the computation of the mean gravity anomalies. In the first method, a planar approximation recently developed by Goyal et al. (2020) is used. The second one is the tesseroidal approximation which is developed by Heck and Seitz (2007). Both methods are inter-compared on grid points. According to differences between both methods; minimum, mean, maximum, and standard deviation of the differences of terrain corrections are − 3.823, − 0.140, 0.961, and 0.538 mGal, respectively. At grid points, the tesseroidal approximation and spatial distribution of differences among both methods are depicted in Fig. 4.

Third, two free-air gravity anomaly grids were computed considering topographic-isostatic reduction as well. For this purpose, topographic-isostatic effects δg^{TI} at the points are computed by spherical harmonic coefficients (Grombein et al. 2014b) and for comparison by applying the Airy-Heiskanen isostatic approach in the space domain. Then, these values are subtracted from free-air gravity anomalies. Subsequently, the reduced anomalies are gridded using the same interpolation technique and options. Finally, a free-air gravity anomaly grid was produced by adding topographic-isostatic values at grid points δg^{I}_{ij} by spherical harmonics to gridded reduced values (see Eq. (11)) as well as in the space domain by forward modelling the effect caused by the isostatic masses.

The resulting variants of the gravity effect at the gravity points are presented in Table 2. The consistently positive, high orthometric terrain heights (see Fig. 1) lead to the large free-air reductions. A very good agreement between the effect of the planar Bouguer plate and the spherical cap can be deduced from the statistical parameters listed in Table 2. The

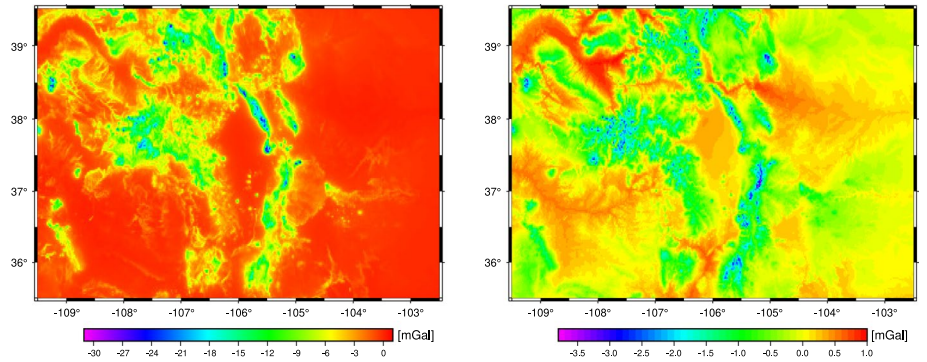

(a) Terrain effects obtained from tesseroidal approximation

(b) Differences between planar and tesseroidal approximations

Fig. 4 Comparison of terrain effects

Table 2 Gravity effects at the 59,303 gravity points. The statistics are in mGal

Effects	Min	Max	Mean	RMS	STD
Remove effects					
Free-air reduction	293.293	1357.593	655.560	679.339	178.169
Planar Bouguer plate	103.668	371.318	232.270	235.833	40.843
Spherical Bouguer cap	105.184	372.817	233.669	237.202	40.785
Spherical Bouguer shell	236.044	857.748	469.955	480.691	101.026
TOPO synthesised	305.420	621.116	438.191	442.825	63.893
ISOS synthesised	− 491.667	− 308.433	− 424.559	426.402	39.604
TOPI+ISO synthesised	− 63.855	132.953	13.632	36.038	33.360
Tesseroidal terrain correction	− 101.577	0.230	− 3.032	5.553	4.652
Topographic effect (tesseroids)	55.967	335.461	230.638	233.913	39.006
Isostatic effect (A-H, tesseroids)	− 257.504	− 94.698	− 192.703	196.287	37.339
Topo+iso effect (tesseroids)	− 124.188	102.141	37.935	40.971	15.477
Free-air anomaly	− 165.475	213.271	5.586	38.739	38.334
Molodensky anomaly	− 165.679	211.938	5.254	38.532	38.173

application of a global spherical shell causes to a large effect, as can be concluded from Eq. (6). It is not considered further for the regional geoid determination. As theoretically expected, the free-air anomaly and the Molodensky gravity anomaly agree very well.

For restoring gravity effects on grids, all statistics of these components are listed in Table 3 and graphically illustrated in Figs. 5 and 6. According to figures, all components completely depend on the topography data. It is not surprising that the statistics of the corresponding effects in the gravity measurement points and the grid points are not identical, which is suggested by the point distribution given in Fig. 2. However, the terrain effects agree very well whether it is calculated in planar approximation or on the tesseroid approach (Heck and Seitz 2007).

Table 3 Block-mean gravity effects on the computation grid (100,000 grid elements). The statistics are in mGal

Effects	Min	Max	Mean	RMS	STD
Restore effects					
Planar Bouguer plate	106.729	458.184	225.889	236.051	68.514
Spherical Bouguer cap	107.802	458.251	227.269	237.352	68.446
Spherical Bouguer shell	213.426	915.779	451.623	471.925	136.932
Planar terrain correction	− 28.901	0.030	− 2.495	3.645	3.168
Tesseroidal terrain correction	− 31.474	0.246	− 2.144	3.845	3.191
Isostatic effect (A-H, tesseroids)	− 257.418	− 94.724	− 175.664	180.336	40.781
Topographic effect (tesseroids)	107.784	438.748	225.125	234.619	66.065
Topo+iso effect (tesseroids)	− 32.067	211.616	49.461	60.390	34.650
Harmonic synthesis					
TOPO	304.911	668.176	424.281	430.450	72.620
ISOS	− 496.806	− 308.587	− 406.034	408.870	48.073
TOIS = TOPO+ISOS	− 80.523	200.832	18.247	42.031	37.864

Finally, all these gravity anomaly grids obtained from different approximations were computed on the grid centres. Statistics of free-air gravity anomalies obtained from different approximation are supplied in Table 4. Figures 5 and 6 show the topographic and isostatic effects generated by gravity forward modelling and synthesis, respectively. There is a good agreement in the long-wavelength signal components, as expected. This is also underlined by the corresponding statistical parameters in Table 4. The isostatic reduction according to Airy-Heiskanen calculated with tesseroids gives very slightly smoothed and centred block-mean free-air gravity anomalies.

Referencing the complete Bouguer gravity anomalies, all grids are inter-compared and the numerical results are represented in Table 5. According to Table 5, topographic-isostatic methods give large differences compared to the complete Bouguer approximation, which means that these methods do not properly represent the topographic anomaly. The spatial distributions of the gravity anomaly differences with respect to the complete Bouguer anomalies via tesseroidal TC are seen in Fig. 7. Topographic-isostatic models disagree from the others due to low resolutions representation of topography.

4.3 Comparison of Geoid Models

Six geoid models called Colorado Geoid based on SB, CB, and TI were computed separately from the boundary data listed in Table 4. During the geoid computations, the LSMSSOFT developed by Abbak and Ustun (2015) was used in this study although several precise geoid modelling methods such as Stokes–Helmert (e. g. Abbak et al. 2024) are available in literature. The LSMSSOFT requires GGM, elevation grid, and free-air anomaly grid as well as some parameters such as capsize (ψ_0), maximum degree (M) of expansion of the GGM, variance of terrestrial gravity data (C_0). In order to compute a precise geoid model, optimum parameters should be determined. Several dozens of "trail and error" are necessary to find the optimum parameters for the project area in question. Once the optimum parameters have been found for the study area, the whole parameters and data files are fixed, except a free-air gravity anomaly grid in each geoid

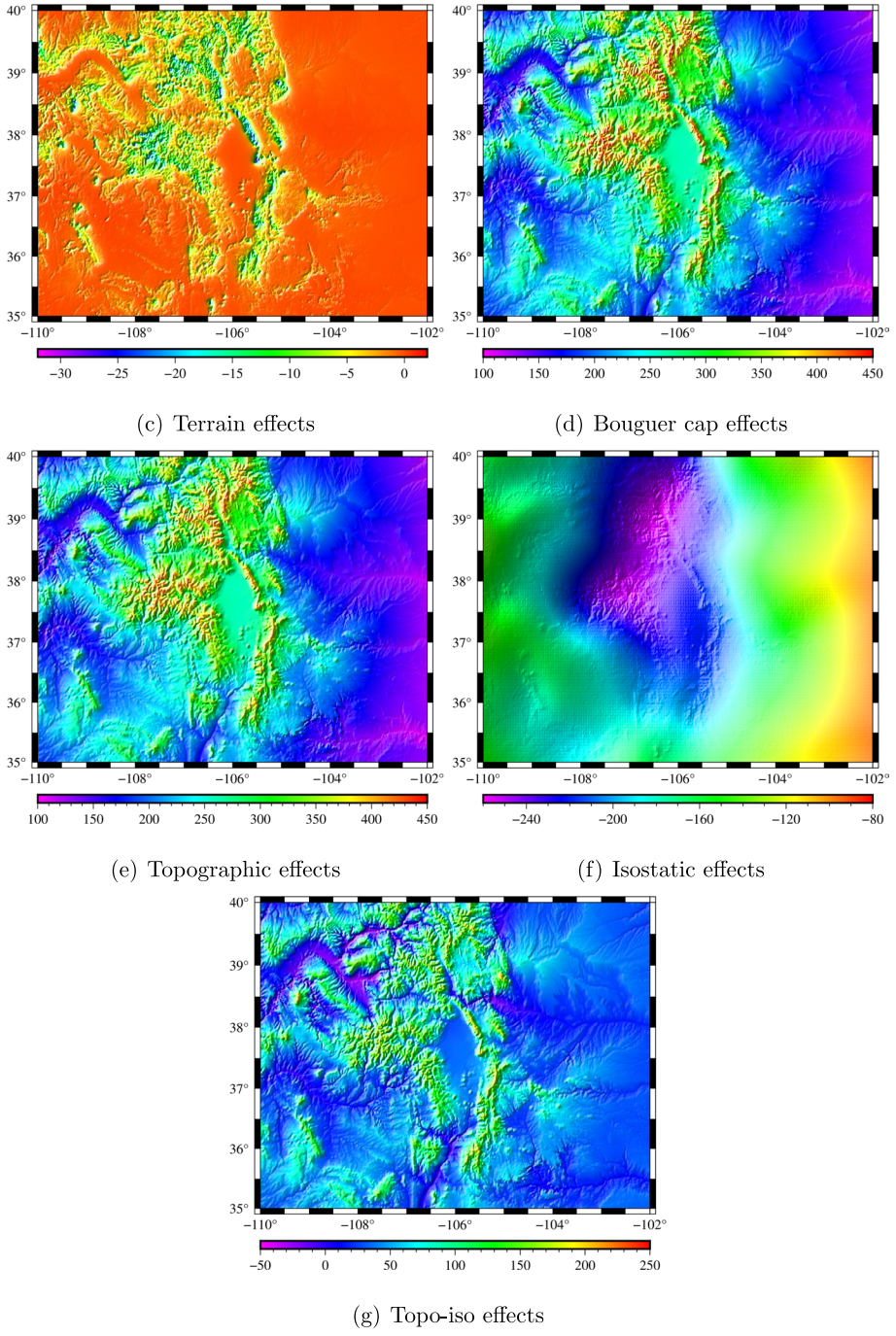

(c) Terrain effects

(d) Bouguer cap effects

(e) Topographic effects

(f) Isostatic effects

(g) Topo-iso effects

Fig. 5 Terrain-, Bouguer cap, isostatic-, top-iso effects obtained from tesseroidal mass discretization

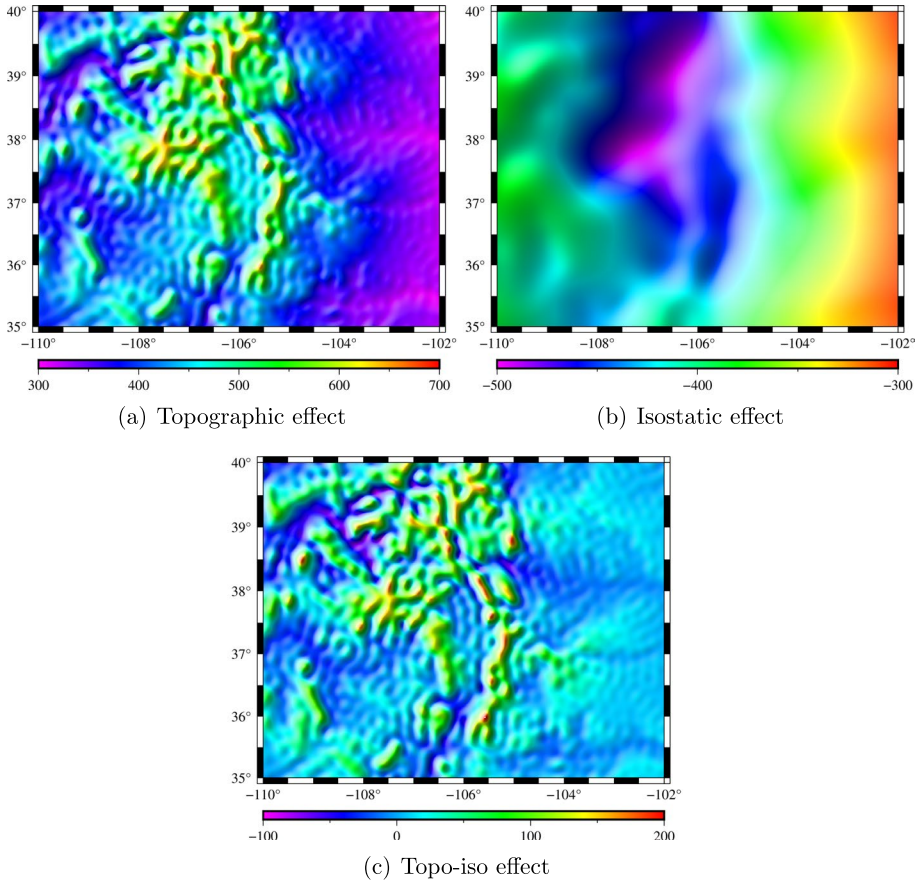

Fig. 6 Topographic-isostatic effects obtained from synthesis of the RWI-model TOIS_2012 (Grombein et al. 2014b)

Table 4 Block-mean free-air gravity anomalies obtained from all approximations. The statistics are in mGal

Gridding types	Min	Max	Mean	STD
Simple Planar Bouguer (SPB)	− 89.295	196.654	17.012	37.969
Simple Cap Bouguer (SCB)	− 89.312	196.362	17.006	37.949
Complete Bouguer via planar TC (CPB)	− 90.024	196.792	17.178	38.123
Complete Bouguer via tesseroidal TC (CTB)	− 89.183	197.218	18.408	38.521
Topographic-Isostatic (RWI_2012) TIM	− 100.866	197.634	14.848	37.675
Topographic-Isostatic (Airy-Heiskanen) TIA	− 100.659	172.975	14.013	35.487

computation. The numerical ranges of all geoid models are listed Table 6. According to the table, all geoid models are giving similar results. Considering the rigorous terrain correction, the geoid model obtained from the complete Bouguer anomalies as boundary data are referenced and subtracted from the other versions. For comparison of the

Table 5 Comparison of mean free-air gravity anomalies with respect to Complete Bouguer anomalies via tesseroidal TC. The statistics are in mGal

Comparison types	Min	Max	Mean	STD
SPB–CTB	− 35.042	19.815	− 1.396	2.416
SCB–CTB	− 35.105	19.312	− 1.403	2.383
CPB–CTB	− 33.081	1.687	− 1.230	1.427
TIM–CTB	− 139.807	94.271	− 3.560	11.589
TIA–CTB	− 130.998	85.603	− 4.395	12.725

geoid solutions in the space domain, their differences are compared with one another in Fig. 8.

It is noteworthy here that in the KTH method the approximate geoid height and downward continuation correction are directly related with the free-air gravity anomaly grid whereas other components (i. e. topographic, atmospheric, and ellipsoidal corrections) does not need a free-air gravity anomaly grid.

As it can be seen from Table 7, the geoid heights for the six elaborated geoid variants, abbreviated by SPB, SCB, CPB and CTB, are in agreement of less than 4 cm (STD). There are large difference of about 25 cm compared to the solutions that include the isostatic effect for smoothing when interpolating the gravity anomalies. This is also illustrated in Fig. 8.

Paying attention to accuracies of geoid models, all of them were tested with GNSS-levelling data (i. e. geometric geoid) in both absolute and relative sense. In geodetic literature, it is not preferred that two kinds of geoid information are directly compared by simply creating the difference between two solutions (e. g. Krdžalić and Abbak 2023). Thus, 5-parameter corrector surface model, including vertical shift, tilting and curvature parameters, was employed during the comparison (see for formulae Pa'suya et al. 2024). Examining the statistical values in Table 8, it can be concluded that the most accurate geoid model elaborated in this study, is based upon free-air gravity anomaly via the complete Bouguer with tesseroidal terrain correction, which means that the tesseroidal terrain corrections precisely represent the gravity field of the topographic masses. The residuals in the GNSS-levelling control points supply a STD of 29 mm and a relative error of 0.84 ppm. On the other hand, topographic-isostatic models disagree so much from the others due to low resolution representation of topography.

5 Conclusion and Remarks

The present study briefly reviews the fundamental theory of the smoothing methods (simple and complete Bouguer anomalies as well as topographic-isostatic reductions) to construct the mean gravity anomaly grids prior to the geoid modeling study. Then, these methods are rigorously applied to the Colorado (USA) test bed, to make comparisons for geoid determination. Following that, these gridded gravity anomalies are successfully included to the computation of a precise geoid model, using the KTH method. All numerical results are inter-compared and externally assessed based on the given GNSS-levelling points.

The main objective is to investigate the effect of different gravity reductions on the determination of block-mean gravity anomalies, which are included in the Stokes integral. It is in the focus of the paper how these gravity anomalies affect the solved geoid, especially in a high mountainous area like the Colorado test area. According to our numerical

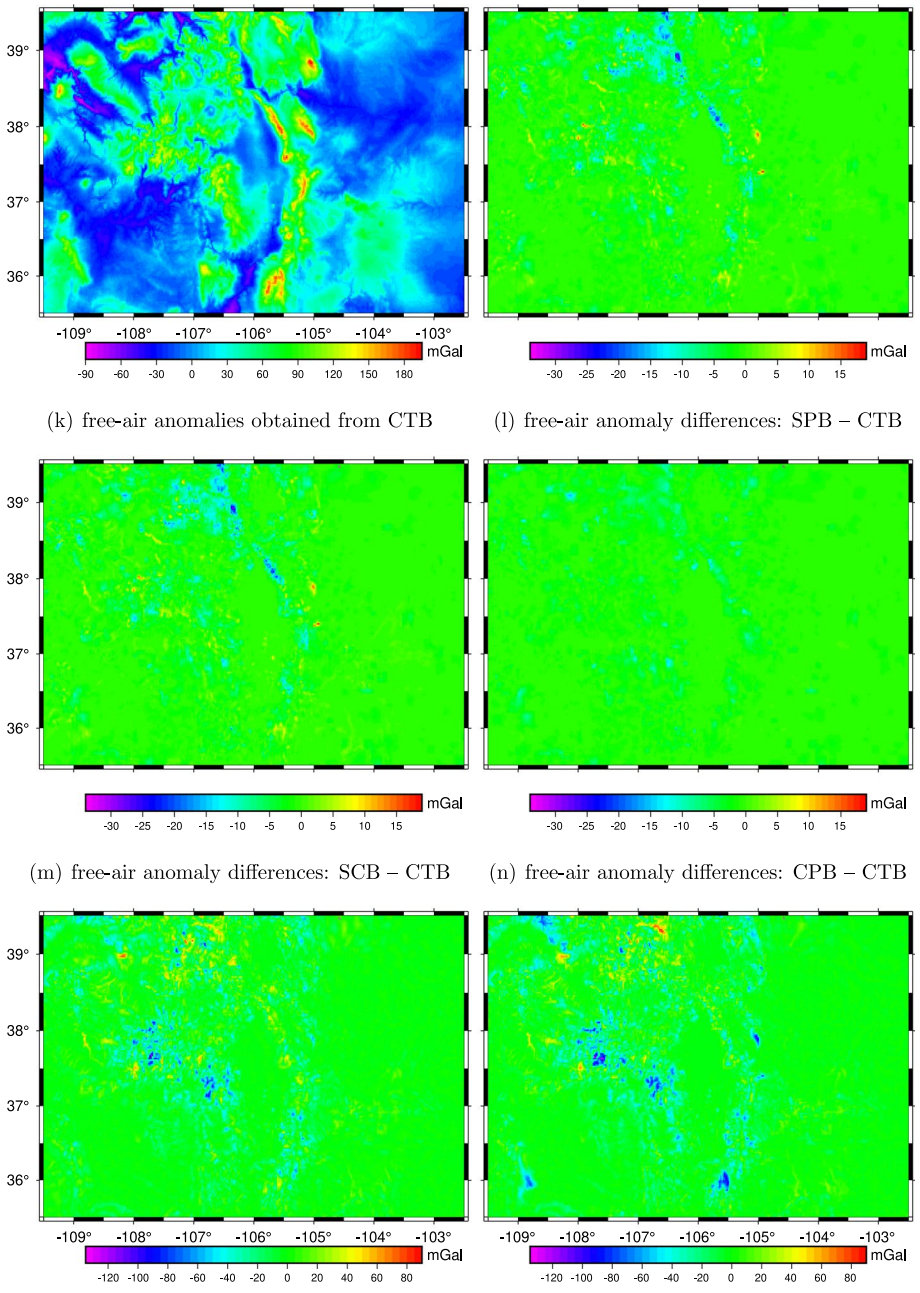

(k) free-air anomalies obtained from CTB

(l) free-air anomaly differences: SPB – CTB

(m) free-air anomaly differences: SCB – CTB

(n) free-air anomaly differences: CPB – CTB

(o) free-air anomaly differences: TOIS – CTB

(p) free-air anomaly differences: A-H – CTB

Fig. 7 Comparison of free-air gravity anomalies

Table 6 Geoid models obtained from all approximations. The statistics are in m

Gridding types	Abbrev.	Min	Max	Mean	STD
Simple Planar Bouguer	SPB	− 20.916	− 13.891	− 16.879	1.779
Simple Cap Bouguer	SCB	− 20.916	− 13.892	− 16.880	1.778
Complete Bouguer via planar TC	CPB	− 20.919	− 13.859	− 16.871	1.789
Complete Bouguer via tesseroidal TC	CTB	− 20.878	− 13.715	− 16.805	1.802
Topographic-Isostatic (RWI_2012)	TIM	− 20.963	− 13.741	− 17.131	1.731
Topographic-Isostatic (Airy-Heiskanen)	TIA	− 20.969	− 13.838	− 17.191	1.707

Table 7 Comparison of geoid models with respect to the one based on complete Bouguer anomalies via tesseroidal TC. The units are in m

Geoid differences	Min	Max	Mean	STD
SPB–CTB	− 0.3572	0.1270	− 0.0738	0.0417
SCB–CTB	− 0.3538	0.1197	− 0.0751	0.0419
CPB–CTB	− 0.2213	0.0189	− 0.0656	0.0269
TOIS–CTB	− 2.0536	0.3809	− 0.3256	0.2687
A-H–CTB	− 2.2008	0.1587	− 0.3863	0.2981

investigations, the maximum difference between the computed geoid models reaches up to 2.05 m, and is highly correlated with elevation, particularly along the northern part of the study area. Comparisons with GNSS-levelling data indicates that there are significant differences between the computed geoid models when isostatic reductions is also applied. If no isostatic reduction is involved during the smoothing process, the geoid solutions are identical to 1 cm level after applying a fitting to GNSS-levelling points. It can be inferred, that the complete Bouguer gravity anomalies (with tesseroidal terrain corrections) should be used in gridding gravity anomalies, particularly in mountainous areas.

In this study, the gridding of gravity anomalies was performed using the near-neighbour method available in the GMT software. As it is well-known, the choice of interpolation technique can introduce additional errors to the computed mean gravity anomalies. Therefore, for achieving a more precise geoid model in this test area, it is recommended to explore and employ a more rigorous interpolation technique (e. g. Least Squares Collocation) to generate mean gravity anomalies.

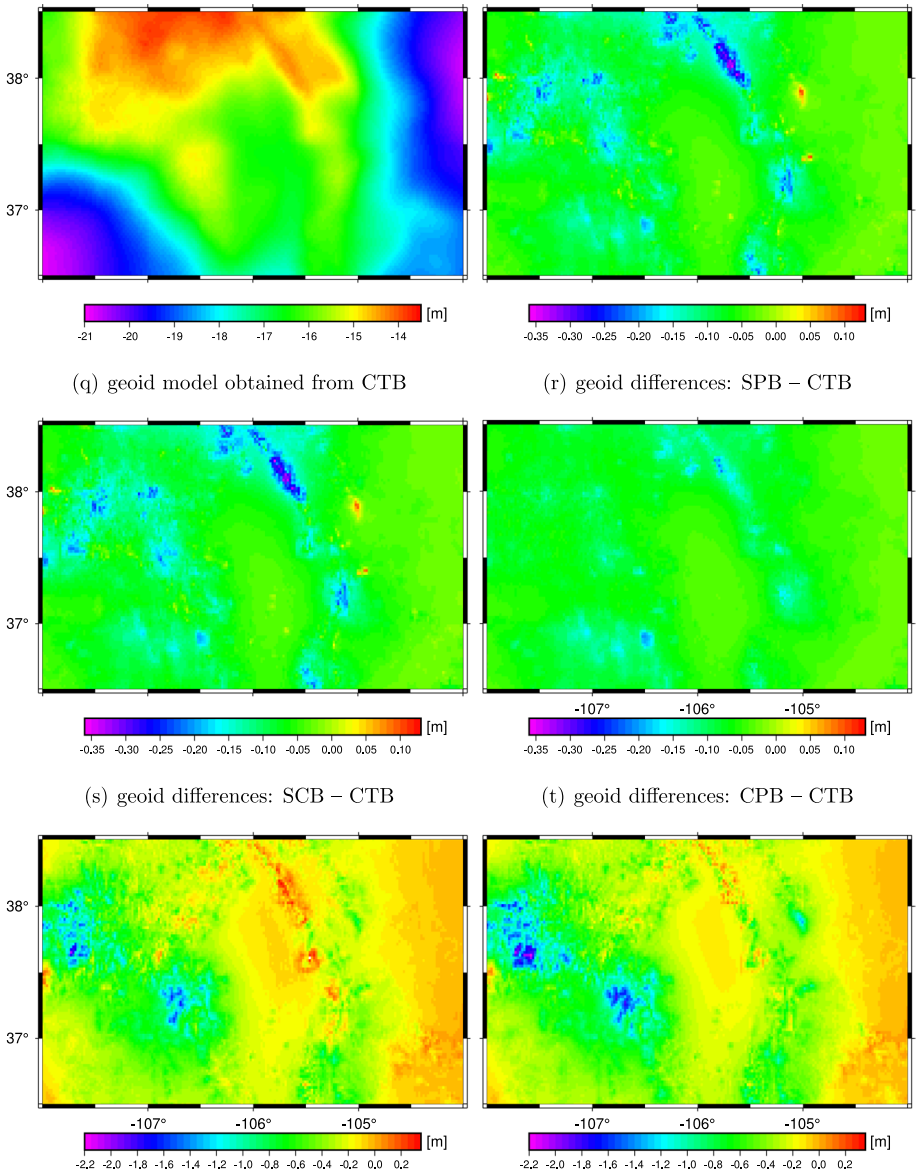

(q) geoid model obtained from CTB

(r) geoid differences: SPB – CTB

(s) geoid differences: SCB – CTB

(t) geoid differences: CPB – CTB

(u) geoid differences: TOIS – CTB

(v) geoid differences: A-H – CTB

Fig. 8 Comparison of the elaborated geoid models

Table 8 The absolute and relative assessments of geoid models in terms of GNSS-levelling data

Geoid models	Absolute assessment			RMS	Relative assessment		
	Min	Max	Mean		Min	Max	Mean
SB planar approx. (before fit)	− 129.25	− 100.00	− 121.25	4.22	0.00	53.38	1.15
SB planar approx. (after fit)	− 8.33	9.88	0.00	3.47	0.00	53.96	1.10
SB spherical approx. (before fit)	− 129.18	− 100.00	− 121.08	4.26	0.00	53.38	1.15
SB spherical approx. (after fit)	− 8.26	9.72	0.00	3.46	0.00	53.88	1.10
CB via planar TC (before fit)	− 130.50	− 100.00	− 122.21	3.23	0.00	52.23	0.97
CB via planar TC (after fit)	−6.19	10.16	0.00	3.01	0.00	52.61	0.94
CB via tesseroidal TC (before fit)	− 140.23	− 100.00	− 128.94	3.11	0.00	54.76	0.88
CB via tesseroidal TC (after fit)	− 5.42	11.28	0.00	**2.93**	0.00	54.67	**0.84**
TI via RWI_2012 (before fit)	− 117.70	− 43.95	− 88.35	21.95	0.00	98.54	3.82
TI via RWI_2012 (after fit)	−21.90	20.08	0.00	8.67	0.00	98.62	3.31
TI via Airy-Heiskanen (before fit)	− 113.35	− 39.04	− 82.50	22.39	0.00	95.45	4.03
TI via Airy-Heiskanen (after fit)	− 26.96	26.18	0.00	9.99	0.00	95.85	3.63

The RMS indicates root mean square error. The absolute assessment is presented in cm, while the relative assessment is expressed in ppm

The bold numbers show the most precise results of gravimetric geoid model after fitting

Acknowledgements During the compilation of the article, the first author was funded by a grant from the Türkiye Scientific and Technology Council (TUBITAK) while he was a visiting professor in the Geodetic Institute at the Karlsruhe Institute of Technology in Germany in 2024. Additionally, the authors would like to thank the state of Baden-Württemberg (Germany) and the Steinbuch centre for Computing at the Karlsruhe Institute of Technology for the allocation of computing time on the high performance parallel computer system.

Author Contributions Ramazan Alpay Abbak designed the study, encoded the LSMSSOFT software, has summarised the differences between the various models, and drafted the initial manuscript. Kurt Seitz elaborated the topographic and isostatic effects based on the tesseroid approach, performed the analyses, and investigated the results. Both authors read, reviewed, and approved the final version of the manuscript.

Funding Open access funding provided by the Scientific and Technological Research Council of Türkiye (TÜBİTAK).

Data Availability The terrestrial gravity and GNSS-levelling data in this study are available at https://www.isgeoid.polimi.it/Projects/colorado_experiment.html while GGMs are downloaded from ICGEM webpage (Ince et al. 2019).

Declarations

Conflict of interest The authors declare that they have no known competing financial interests or personal relationships that could have appeared to influence the work reported in this paper.

References

Abbak RA, Ustun A (2015) A software package for computing a regional gravimetric geoid model by the KTH method. Earth Sci Inf 8(1):255–265

Abbak RA, Ellmann A, Ustun A (2022) A practical software package for computing gravimetric geoid by the least squares modification of Hotine's formula. Earth Sci Inf 1(15):713–724

Abbak RA, Goyal R, Ustun A (2024) A user-friendly software package for modelling gravimetric geoid by the classical Stokes–Helmert method. Earth Sci Inf 17(4):3811–3824

Abd-Elmotaal HA, Kühtreiber N, Seitz K, Heck B (2020) The new afrgdb_v2. 2 gravity database for Africa. Pure Appl Geophys 177(9):4365–4375

Ågren J, Sjöberg LE, Kiamehr R (2009) The new gravimetric quasi geoid model KTH08 over Sweden. J Appl Geodesy 3:143–153

Bildirici I, Ustun A, Ulugtekin N, Selvi HZ, Abbak R, Bugdayci I, Dogru AO (2007) SRTM data in Turkey: void filling strategy and accuracy assessment. In: The 4th Middle East spatial technology (MEST) conference and exhibition, pp 10–12

Bildirici I, Ustun A, Ulugtekin N, Selvi HZ, Abbak R, Bugdayci I, Dogru AO (2008) Comparison of SRTM and 25K topographic maps in Turkey. In: The second international conference on cartography and GIS, January 21–24, Borovets, Bulgaria

CGE (2025) Colorado 1 cm geoid experiment. https://geodesy.noaa.gov/GEOID/research/co-cm-experiment. Accessed on 18 Jan 2025

Farr TG, Rosen PA, Caro E, Crippen R, Duren R, Hensley S, Kobrick M, Paller M, Rodriguez E, Roth L et al (2007) The shuttle radar topography mission. Rev Geophys 45(2):1

Featherstone W (2003) Software for computing five existing types of deterministically modified integration kernel for gravimetric geoid determination. Comput Geosci 29(2):183–193

Featherstone W, Kirby J (2000) The reduction of aliasing in gravity anomalies and geoid heights using digital terrain data. Geophys J Int 141(1):204–212

Forsberg R (1984) A study of terrain reductions, density anomalies and geophysical inversion methods in gravity field modelling. Department of Geodetic Science and Surveying, Report 355, Ohio State University, Columbus, Ohio, USA

Forsberg R, Tscherning CC (1997) Topographic effects in gravity field modelling for BVP. In: Sansò F, Rummel R (eds) Geodetic boundary value problems in view of the one centimeter geoid, vol 65. Lecture notes in Earth sciences. Springer, Berlin, pp 239–272

Forsberg R, Tscherning CC (2014) An overview manual for the GRAVSOFT geodetic gravity field modelling programs, 3rd edn. National Space Institute, Denmark

Goos J, Featherstone W, Kirby J, Holmes S (2003) Experiments with two different approaches to gridding terrestrial gravity anomalies and their effect on regional geoid computation. Surv Rev 37(288):92–112

Goyal R, Featherstone W, Tsoulis D, Dikshit O (2020) Efficient spatial-spectral computation of local planar gravimetric terrain corrections from high-resolution digital elevation models. Geophys J Int 221(3):1820–1831

Grombein T, Seitz K, Heck B (2013) Optimized formulas for the gravitational field of a tesseroid. J Geodesy 87(7):645–660

Grombein T, Luo X, Seitz K, Heck B (2014a) A wavelet-based assessment of topographic-isostatic reductions for GOCE gravity gradients. Surv Geophys 35:959–982

Grombein T, Seitz K, Heck B (2014b) Rock–Water–Ice topographic-isostatic gravity field model 2012 (RWI 2012 model). Accessed on 18 Jan 2025

Heck B (1988) On the non-linear geodetic boundary value problem for a fixed boundary surface. Bull Géodésique 62:57–67

Heck B, Seitz K (2003) Solutions of the linearized geodetic boundary value problem for an ellipsoidal boundary to order e^3. J Geodesy 77(3):182–192

Heck B, Seitz K (2007) A comparison of the tesseroid, prism and point-mass approaches for mass reductions in gravity field modelling. J Geodesy 81:121–136

Heiskanen WA, Moritz H (1967) Physical geodesy. W. H. Freeman and Company, San Francisco

Hofmann-Wellenhof B, Moritz H (2006) Physical geodesy. Springer, Berlin

Ince ES, Barthelmes F, Reißland S, Elger K, Förste C, Flechtner F, Schuh H (2019) ICGEM-15 years of successful collection and distribution of global gravitational models, associated services, and future plans. Earth Syst Sci Data 11(2):647–674

Işık MS, Erol B, Erol S, Sakil FF (2021) High-resolution geoid modeling using least squares modification of Stokes and Hotine formulas in Colorado. J Geodesy 95(5):49

Jalal SJ, Musa TA, Din AHM, Wan Aris WA, Pa'suya MF (2022) Improving the accuracy of local gravimetric geoid modelling using simulated terrestrial gravity data. Pure Appl Geophys 179(8):2869–2887

Janák J, Vaníček P (2005) Mean free-air gravity anomalies in the mountains. Stud Geophys Geod 49(1):31–42

Kadlec M (2011). Refining gravity field parameters by residual terrain modelling. PhD thesis, Faculty of Applied Sciences, University of West Bohemia, Pizen

Krdžalić D, Abbak RA (2023) A precise geoid model of Bosnia and Herzegovina by the KTH method and its validation. Surv Rev 55(393):513–523

Kuhn M (2003) Geoid determination with density hypotheses from isostatic models and geological information. J Geodesy 77:50–65

Lemoine FG, Factor SCKJK, Pavlis RTNK, Chinn DS, Cox CM, Klosko SM, Luthcke SB, Torrence MH, Wang YM, Pavlis RGWEC, Rapp RH, Olson TR (1998) The Development of the Joint NASA GSFC and NIMA Geopotential Model EGM96. Report, NASA Goddard Space Flight Center, Greenbelt, Maryland, USA

Lu B, Luo Z, Zhong B, Zhou H, Flechtner F, Förste C, Barthelmes F, Zhou R (2018) The gravity field model IGGT_R1 based on the second invariant of the GOCE gravitational gradient tensor. J Geodesy 92:561–572

Mader K (1951) Das Newtonsche Raumpotential prismatischer Körper und seine Ableitungen bis zur dritten Ordnung. Österreichische Zeitschrift für Vermessungswesen, Sonderheft, vol 11

Marotta A, Barzaghi R (2017) A new methodology to compute the gravitational contribution of a spherical tesseroid based on the analytical solution of a sector of a spherical zonal band. J Geodesy 91(10):1207–1224

Marotta AM, Seitz K, Barzaghi R, Grombein T, Heck B (2019) Comparison of two different approaches for computing the gravitational effect of a tesseroid. Stud Geophys Geod 63(5):321–344

Moritz H (1980a) Advanced physical geodesy. Wichmann, Karlsruhe

Moritz H (1980b) Geodetic reference system 1980. Bull Géodésique 54(3):395–405

Nagy D, Papp G, Benedek J (2002) Corrections to "The gravitational potential and its derivatives for the prism''. J Geodesy 76(8):475

Nergizci M, Abbak RA, Arisoy MO (2024) The effect of crustal density heterogeneity on determining gravimetric geoid: example in Central Anatolia. Türk J Asian Earth Sci 264:106037

Olgun S, Üstün A, Akyılmaz O (2023) tc-cylinder: an optimized algorithm for accurate topography effect from high-resolution digital elevation models. Comput Geosci 170:105264

Pa'suya MF, Din AHM, Abbak RA, Talib N, Aziz MAC, Ramli MZ, Hamden MH, Yazid NM (2024) Integration of local mean sea level and land vertical datum over Peninsular Malaysia via transformation model. Pure Appl Geophys 181(2024):3703–3721

Sansò F, Rummel R (1997) Geodetic boundary value problems in view of the one centimeter geoid, vol 65. Lecture notes in earth sciences, Springer

Seitz K, Heck B, Abd-Elmotaal H (2023) External gravitational field of a homogeneous ellipsoidal shell: a reference for testing gravity modelling software. J Geodesy 97(54):1–18

Sjöberg L (1984) Least-squares modification of Stokes' and Vening–Meinez' formula by accounting for truncation and potential coefficients errors. Manusc Geod 9:209–229

Sjöberg L (1991) Refined least squares modification of Stokes' formula. Manuscr Geodaet 16(6):367–375

Sjöberg LE (1998) The exterior Airy/Heiskanen topographic–isostatic gravity potential, anomaly and the effect of analytical continuation in Stokes' formula. J Geodesy 72(11):654–662

Sjöberg LE (2003) A general model for modifying Stokes' formula and its least-squares solution. J Geodesy 77:459–464

Sjöberg LE (2009) The terrain correction in gravimetric geoid computation-is it needed? Geophys J Int 176(1):14–18

Somigliana C (1929) Teoria del campo gravitazionale dell'ellissoide di rotazione. Mem Soc Astron Ital 4:1

Somigliana C (1930) Sul campo gravitationale esterno del geoide ellissoidico. Atti Accad Lincei V I(11):237–243

Ustun A, Bildirici IO, Selvi HZ, Abbak RA (2006) An evaluation of SRTM3 DTM data: validity, problems and solutions. In: The first international conference on cartography and GIS, Borovets, Bulgaria

van Westrum D, Ahlgren K, Hirt C, Guillaume S (2021) A Geoid Slope Validation Survey (2017) in the rugged terrain of Colorado, USA. J Geodesy 95:1–19

Vaníček P, Tenzer R, Sjöberg LE, Martinec Z, Featherstone WE (2004) New views of the spherical bouguer gravity anomaly. Geophys J Int 159(2):460–472

Wang YM, Sánchez L, Ågren J, Huang J, Forsberg R, Abd-Elmotaal HA, Ahlgren K, Barzaghi R, Bašić T, Carrion D et al (2021) Colorado geoid computation experiment: overview and summary. J Geodesy 95:1–21

Wessel P, Luis J, Uieda L, Scharroo R, Wobbe F, Smith WH, Tian D (2019) The generic mapping tools version 6. Geochem Geophys Geosyst 20(11):5556–5564